



## Regional pollen-based Holocene temperature and precipitation patterns depart from the Northern Hemisphere mean trends

Ulrike Herzschuh<sup>1,2,3</sup>, Thomas Böhmer<sup>1</sup>, Manuel Chevalier<sup>4,5,6</sup>, Anne Dallmeyer<sup>5</sup>, Chenzhi Li<sup>1,2</sup>,  
5 Xianyong Cao<sup>1,7</sup>, Raphaël Hébert<sup>1</sup>, Odile Peyron<sup>8</sup>, Larisa Nazarova<sup>1,9</sup>, Elena Y. Novenko<sup>10,11</sup>,  
Jungjae Park<sup>12,13</sup>, Natalia A. Rudaya<sup>14,15</sup>, Frank Schlütz<sup>16,17</sup>, Lyudmila S. Shumilovskikh<sup>17</sup>,  
Pavel E. Tarasov<sup>18</sup>, Yongbo Wang<sup>19</sup>, Ruilin Wen<sup>20,21</sup>, Qinghai Xu<sup>22</sup>, Zhuo Zheng<sup>23,24</sup>

<sup>1</sup> Alfred Wegener Institute Helmholtz Centre for Polar and Marine Research, Polar Terrestrial Environmental Systems, Telegrafenberg A45, 14473 Potsdam, Germany

10 <sup>2</sup> Institute of Environmental Science and Geography, University of Potsdam, Karl-Liebknecht-Str. 24-25, 14476 Potsdam, Germany

<sup>3</sup> Institute of Biochemistry and Biology, University of Potsdam, Karl-Liebknecht-Str. 24-25, 14476 Potsdam, Germany

15 <sup>4</sup> Institute of Geosciences, Sect. Meteorology, Rheinische Friedrich-Wilhelms-Universität Bonn, Auf dem Hügel 20, 53121 Bonn, Germany

<sup>5</sup> Max Planck Institute for Meteorology, Bundesstrasse 53, 20146 Hamburg, Germany

<sup>6</sup> Institute of Earth Surface Dynamics IDYST, Faculté des Géosciences et l'Environnement, University of Lausanne, Batiment Géopolis, 1015 Lausanne, Switzerland

20 <sup>7</sup> Alpine Paleocology and Human Adaptation Group (ALPHA), State Key Laboratory of Tibetan Plateau Earth System, Resources and Environment (TPESRE), Institute of Tibetan Plateau Research, Chinese Academy of Sciences, 100101 Beijing, China

<sup>8</sup> Institut des Sciences de l'Evolution de Montpellier, Université de Montpellier, CNRS UMR 5554, Montpellier, France

<sup>9</sup> Kazan Federal University, Kremlyovskaya str. 18, 420008 Kazan, Russia

25 <sup>10</sup> Lomonosov Moscow State University, Faculty of Geography, Leniskie gory 1, 119991 Moscow, Russia

<sup>11</sup> Department of Quaternary Paleogeography, Institute of Geography Russian Academy of Science, Staromonrtny lane, 29, 119017, Moscow, Russia

<sup>12</sup> Department of Geography, Seoul National University, 1 Gwanak-ro, Gwanak-gu, Seoul, 08826, Republic of Korea

30 <sup>13</sup> Institute for Korean Regional Studies, Seoul National University, 1 Gwanak-ro, Gwanak-gu, Seoul, 08826, Republic of Korea



<sup>14</sup> PaleoData Lab, Institute of Archaeology and Ethnography, Siberian Branch, Russian Academy of Sciences, Pr. Akademika 36 Lavrentieva 17, 630090 Novosibirsk, Russia

<sup>15</sup> Biological Institute, Tomsk State University, Pr. Lenina, 26, Tomsk, 634050, Russia

35 <sup>16</sup> Lower Saxony Institute for Historical Coastal Research, D-26382 Wilhelmshaven, Germany

<sup>17</sup> Department of Palynology and Climate Dynamics, Albrecht-von-Haller Institute for Plant Sciences, University of Göttingen, Untere Karspüle 2, 37073 Göttingen, Germany

<sup>18</sup> Freie Universität Berlin, Institute of Geological Sciences, Palaeontology Section, Malteserstrasse 74-100, Building D, 12249 Berlin, Germany

40 <sup>19</sup> College of Resource Environment and Tourism, Capital Normal University, 105 West 3rd Ring Rd N, 100048 Beijing, China

<sup>20</sup> Key Laboratory of Cenozoic Geology and Environment, Institute of Geology and Geophysics, Chinese Academy of Sciences, 19 Beitucheng West Road, Chaoyang District, 100029 Beijing, China

<sup>21</sup> CAS Center for Excellence in Life and Paleoenvironment, 100044 Beijing, China

45 <sup>22</sup> College of Geographical Sciences, Hebei Normal University, 050024 Shijiazhuang, China

<sup>23</sup> Guangdong Key Lab of Geodynamics and Geohazards, School of Earth Sciences and Engineering, Sun Yat-sen University, 519082 Zhuhai, China

<sup>24</sup> Southern Marine Science and Engineering Guangdong Laboratory (Zhuhai), 519082 Zhuhai, China

*Correspondence to:* Ulrike Herzschuh (Ulrike.Herzschuh@awi.de)

50

**Abstract.** A mismatch between model- and proxy-based Holocene climate change, known as the Holocene conundrum, may partially originate from the poor spatial coverage of climate reconstructions in, for example, Asia, limiting the number of grid-cells for model-data comparisons. Here we investigate hemispheric, latitudinal, and regional mean time-series as well as anomaly maps of pollen-based reconstructions of mean annual temperature, mean July temperature, and annual precipitation from 1676 records in the Northern Hemisphere extratropics. Temperature trends show strong latitudinal patterns and differ between (sub-)continents. While the circum-Atlantic regions in Europe and eastern North America show a pronounced mid-Holocene temperature maximum, western North America shows only weak changes and Asia mostly a continuous Holocene temperature increase but with strong latitudinal differences. Likewise, precipitation trends show certain regional peculiarities such as the pronounced mid-Holocene optimum between 30 and 40°N in Asia and Holocene increasing trends in Europe and western North America which can all be linked with Holocene changes of the regional circulation pattern linked to temperature change. Given a background of strong regional heterogeneity, we conclude that the calculation of global or hemispheric means which initiated the Holocene conundrum debate should focus more on understanding the spatio-temporal patterns and their regional drivers.



## 1 Introduction

Previous comparisons of proxy-based reconstructions and simulations of global Holocene climate change have yielded major mismatches, a discrepancy termed the ‘Holocene conundrum’ (Liu et al., 2014c). While simulations indicate an increase in Holocene temperature (Liu et al., 2014c), proxy data syntheses rather support a mid-Holocene optimum (Marcott et al., 2013; Kaufman et al., 2020b). Recently, several explanations for this finding were proposed, most of which assign the mismatch to biases in the proxy data with respect to location or seasonality (Marsicek et al., 2018; Bader et al., 2020; Bova et al., 2021; Osman et al., 2021).

Previous temperature reconstructions from continental areas are mainly available from the circum-North Atlantic region, and are potentially unrepresentative of the whole Northern Hemisphere temperature change, as the region was strongly impacted by the vanishing Laurentide ice-sheet (Rolandone et al., 2003; Chouinard and Mareschal, 2009). Synthesis studies hitherto included only a few records from the large non-glaciated Asian continent despite the existence of many Holocene pollen records (Cao et al., 2019; Herzschuh et al., 2019) and high-quality modern pollen datasets (Tarasov et al., 2011; Cao et al., 2014; Davis et al., 2020; Dugerdil et al., 2021) potentially allowing for higher quality quantitative reconstructions.

While temperature patterns have often been studied, hemispheric syntheses of quantitative precipitation change during the Holocene are not yet available. A recent study of qualitative moisture proxy data suggests an overall warm and dry mid-Holocene in the Northern Hemisphere mid-latitudes, related to the weakened latitudinal temperature gradient (Routson et al., 2019). This trend contrasts with the idea of positive hydrological sensitivity, that is, warm climates are wet at a global scale (Trenberth, 2011), which was confirmed from proxy and model studies from monsoonal areas in lower latitudes (Kutzbach, 1981; Wang et al., 2017). The study of Routson et al. (2019) only included a few records from the subtropical monsoonal Asia that is known for complex Holocene moisture patterns (Herzschuh, 2004; Chen et al., 2019; Herzschuh et al., 2019). These and further synthesis studies (Wang et al., 2010; Chen et al., 2015; Wang et al., 2020) also gave a plethora of alternative explanations to characterize these patterns, including interactions between the monsoon and westerlies circulation and evaporation effects.

Pollen spectra are a well-established palaeoclimate proxy and quantitative estimates of past climatic change are mainly derived by applying (transfer functions of) modern pollen-climate calibration sets to fossil pollen records (Birks et al., 2010; Chevalier et al., 2020). Accordingly, pollen-based reconstructions constitute a substantial part of multi-proxy syntheses (e.g., Kaufman et al., 2020b), but unfortunately, they are derived from different calibration sets and methods, making a consistent assessment of inherent reconstruction biases difficult. Pollen data are one of the few land-derived proxies available that can theoretically contain independent information on both temperature and precipitation in the same record (Chevalier et al., 2020; Mauri et al., 2015). Consistent pollen-based reconstructions can thus contribute to better characterizing past temperature and precipitation changes across large landmasses and how these changes co-vary over time (Davis et al., 2003).

Here we analyze spatio-temporal patterns of pollen-based reconstructions of mean annual temperature ( $T_{\text{ann}}$ ), mean July temperature ( $T_{\text{July}}$ ), and mean annual precipitation ( $P_{\text{ann}}$ ) from 1676 sites from the



Northern Hemisphere extratropics that were generated using harmonized methods and calibration datasets (LegacyClimate 1.0, Herzschuh et al., 2022a) and have revised chronologies (Li et al., 2022). We address the following questions: (1) What are the continental, latitudinal, and regional patterns of Holocene temperature change in the Northern Hemisphere extratropics and how do our new reconstructions align with the global averaged trends of a previous global temperature synthesis? (2) What are the continental, latitudinal, and regional patterns of Holocene precipitation change and how do these changes co-vary with temperature trends?

## 2 Methods

This study analyzes pollen-based reconstructions provided in the LegacyClimate 1.0 dataset (Herzschuh et al., 2022a). It contains pollen-based reconstructions of  $T_{July}$ ,  $T_{ann}$ , and  $P_{ann}$  of 2594 records along with transfer function metadata and estimates of reconstruction errors and is accompanied by a manuscript analyzing reconstruction biases and presenting reliability tests. The fossil pollen records, representing the LegacyPollen 1.0 (Herzschuh et al., 2022b) dataset, originate from Neotoma (last access: July 2020), a dataset from eastern and central Asia (Cao et al., 2013; Herzschuh et al., 2019), a dataset from northern Asia (Cao et al., 2019), and a few additional records. The chronologies of LegacyPollen 1.0 are based on revised chronologies provided by Li et al. (2022). Taxa are harmonized to genus level for woody taxa and major herbaceous taxa and to family level for other herbaceous taxa. Along with LegacyClimate 1.0, a taxonomically harmonized modern pollen dataset is provided (a total of 15,341 samples; Herzschuh et al., 2021) which includes datasets from Europe (EMPD2, Davis et al., 2020), Asia (Tarasov et al., 2011; Herzschuh et al., 2019; Dugerdil et al., 2021), and North America (from Neotoma; Whitmore et al., 2005). LegacyClimate 1.0 also provides the climate data for the sites of the modern pollen samples that were derived from WorldClim 2 (Fick and Hijmans, 2017).

Of the 2594 records available, 1676 records cover at least 4000 years of the Holocene and were included in the time-slice comparisons (Fig. 1). The construction of time-series to estimate the means of climate variables was restricted to those 991 records that cover the full period of 11 to 1 ka.

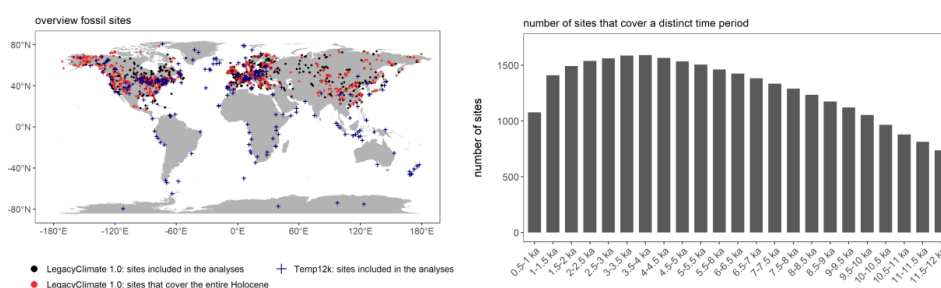


**Figure 1. Temporal and spatial coverage of the LegacyClimate1.0 dataset (dots) and of Temp12K (Kaufman et al. 2020b, crosses) used in this analysis.**

The map shows sites that cover the entire Holocene (i.e., 11-1 ka) as red symbols and those that cover parts of the Holocene but at least 4000 years in the period between 0 and 12 ka as black symbols.



LegacyClimate 1.0 provides reconstructions based on different methodologies including two versions of WA-PLS (weighted averaging partial least squares regression, a transfer function-based approach) and MAT (modern analogue technique). For each fossil site a unique calibration set from modern sites within a 2000 km radius was first set up (Cao et al., 2014). For WA-PLS, the best component, typically first or second, is identified using model statistics as derived from leave-one-out cross-validation (ter Braak and Juggins, 1993). A WA-PLS\_tailored reconstruction set is also provided in the LegacyClimate 1.0 dataset (Herzschuh et al., 2022a). In WA-PLS\_tailored, the modern range of the non-target variable is reduced by tailoring the modern pollen dataset to restrict the impact of precipitation on the temperature reconstruction and vice versa. However, initial assessments did not show any major differences compared to using the standard WA-PLS-derived reconstruction. As such, we do not make use of this dataset for this study to be consistent with previous studies. The MAT reconstructions were derived from the seven best analogues that we identified based on the dissimilarity measures between the fossil samples and the modern pollen assemblages using the squared-chord distance metric (Simpson, 2012). MAT reconstructions were highly correlated with those obtained by WA-PLS (Herzschuh et al., 2022a). Here, we opted for the widely used WA-PLS, as it is less sensitive to the size and environmental gradient length of the modern pollen dataset and is thus less affected by spatial autocorrelation effects and can better handle poor analogue situations (ter Braak and Juggins, 1993; Telford and Birks, 2011; Cao et al., 2014; Chevalier et al., 2020). The mean RMSEP (WA-PLS) from all 991 sites included in the time-series analyses is  $2.48 \pm 0.7^\circ\text{C}$  (one standard deviation) for  $T_{\text{July}}$ ,  $2.64 \pm 0.5^\circ\text{C}$  for  $T_{\text{ann}}$ , and  $242.54 \pm 75.5$  mm for  $P_{\text{ann}}$ . They show a spatial pattern in that the RMSEPs are higher in areas with steep climate gradients (e.g., central Asia and along the western coast of North America, see Fig. 3 in Herzschuh et al., 2022a). As it has already been shown in previous comparisons, WA-PLS can have higher RMSEPs than MAT but these do not necessarily reflect a less reliable reconstruction but methodological differences (Cao et al., 2014). Besides, the reconstruction errors are likely much smaller when only the trends and the relative changes are assessed, as in this study.

Derived time-series of  $T_{\text{July}}$ ,  $T_{\text{ann}}$ , and  $P_{\text{ann}}$  were smoothed over a 500-yr time-scale and resampled at a 100 yr-resolution using the *corit* package in R (version 0.0.0.9000, Reschke et al., 2019). These derived time-series were sampled at selected time-slices and converted into a regular  $2^\circ \times 2^\circ$  raster grid (by taking the mean of all records located within the grid-cell) using the *raster* package in R (version 3.5-11, R Core Team, 2020; Hijmans et al., 2021).  $P_{\text{ann}}$  is presented as % relative to the 1 ka reference period (mean curve) or relative to the younger time-slice (map).

To calculate zonal, (sub-)continental, and hemispheric means we selected all 991 smoothed and resampled time-series of  $T_{\text{July}}$ ,  $T_{\text{ann}}$ , and  $P_{\text{ann}}$  that cover the full period between 11 and 1 ka and converted them into a regular  $2^\circ \times 2^\circ$  raster grid. In total, 437 grid-cells between  $30$  and  $80^\circ\text{N}$  are covered by one or more time-series. The estimate at 1 ka was used as a reference to calculate the anomalies as many records either poorly or do not cover the last 0.5 ka. The mean of climate variable anomalies of all grid-cell curves originating from a zonal band of  $10^\circ$  of a sub-continent (e.g., for  $30$ - $40^\circ\text{N}$  of Europe) were calculated to derive the zonal mean time-series for each sub-continent. Such derived zonal means were weighted by the terrestrial area represented in the zonal band to calculate the mean time-series of the (sub-)continents i.e., Asia, Europe, Eastern North America ( $<105^\circ\text{W}$ ; Williams et al., 2000).



Likewise the area-weighting was applied to derive the continental means and hemispheric-wide (zonal) means. Area calculation was implemented using the *raster* package in R (version 3.5-11, R Core Team, 2020; Hijmans et al., 2021).

180 Furthermore, we extracted the 249 records that cover the full Holocene period in the Temp12k dataset (Kaufman et al., 2020b; instead of 11.0 ka we here used a cut-off of 10.5 ka as many records in this dataset start shortly after 11.0 ka; Fig. 1). Four records were deleted because of extreme Holocene deviations of  $>7^{\circ}\text{C}$  leaving 245 records that were used to construct the mean temperature time-series similar to the approach described for the LegacyClimate1.0 dataset. We excluded all pollen-based  
185 reconstructions from the Temp12k dataset ( $n=111$ ) which are between  $30$  and  $80^{\circ}\text{N}$  and which are already present in the LegacyClimate 1.0 dataset to avoid duplications when integrating both datasets into a joint hemispheric and global mean temperature stack curve.

### 3 Results

#### 190 3.1 Spatio-temporal pattern of temperature reconstructions

The temporal patterns of temperature records covering the entire Holocene (i.e., 11-1 ka) show strong differences between continents (Fig. 2). Europe shows a pronounced mid-Holocene optimum of  $+1.31^{\circ}\text{C}$  for  $T_{\text{July}}$  at 7.2 ka while the  $T_{\text{ann}}$  optimum occurs later and is less pronounced ( $+0.87^{\circ}\text{C}$  at 5.6 ka). The mid-Holocene  $T_{\text{July}}$  was weaker in Eastern North America ( $+0.49^{\circ}\text{C}$ ) while  $T_{\text{ann}}$  warming was in a similar  
195 range  $+0.85^{\circ}\text{C}$  ( $T_{\text{ann}}$ ) to Europe. Asia ( $T_{\text{July}}$ ) and Western North America ( $T_{\text{ann}}$ ) show almost no optimum but only some variations around a continuously increasing Holocene trend, with a higher increase rate before 6 ka than after 6 ka.

Aside from these differences among (sub-)continents, certain regional differences exist. Early Holocene cold climate anomalies were most pronounced in latitudes between  $45^{\circ}\text{N}$  and  $65^{\circ}\text{N}$ , particularly in  
200 Northern Europe, Northeastern Asia, and Alaska (Fig. 3) with above  $2.5^{\circ}\text{C}$  deviation to mean Holocene  $T_{\text{ann}}$  optimum values in most records. The most pronounced  $T_{\text{ann}}$  optimum of  $>+1.5^{\circ}\text{C}$  compared to the late Holocene can be found in Europe north of  $60^{\circ}\text{C}$  and Eastern North America between  $60$  and  $70^{\circ}\text{N}$  forming a circum-North Atlantic pattern (Fig. 4). Records from Eastern Europe, inner Asia, and Southern North America show mostly no mid-Holocene optimum, but rather a late-Holocene optimum. Records  
205 with an early-Holocene optimum dominate the north-central part of North America and China, though these areas are characterized by high spatial variability. High ranges of Holocene temperature variations ( $>5^{\circ}\text{C}$ ) are found in mid-latitude Europe, Western Canada, Southeastern US, and along the north Asian Pacific coast.

The averaged Northern Hemisphere  $>30^{\circ}\text{N}$  time-series of all records that cover the entire Holocene  
210 ( $n=991$ , Fig. 5) indicate that mean  $T_{\text{July}}$  was lowest at the beginning of the Holocene ( $-0.59^{\circ}\text{C}$  compared to present), increased until 7 ka ( $+0.47^{\circ}\text{C}$  compared to present), and slightly decreased afterwards to reach modern temperatures.  $T_{\text{ann}}$  was also lowest at the beginning of the Holocene ( $-1.26^{\circ}\text{C}$  compared to present) and reached its maximum of  $0.29^{\circ}\text{C}$  compared to present at 6.4 ka.



215 Finally, our revised global temperature curve includes all of our records that cover the entire Holocene  
plus all records in the Temp12k dataset (Kaufman et al., 2020b) that cover the entire Holocene and are  
not from identical pollen records (in total, 1129 records). It shows that mean  $T_{ann}$  was lowest during the  
early Holocene at 10.3 ka with a 0.007°C anomaly relative to 1 ka and warmest at 5.1 ka with a warming  
of 0.49°C. For Northern Hemisphere extratropics (30-80°N) we find that mean  $T_{ann}$  was lowest during  
the early Holocene at 10.5 ka with a -0.22°C anomaly relative to 1 ka and warmest at 6.4 ka with a  
220 warming of 0.08°C.

### 3.2 Spatio-temporal pattern of precipitation reconstructions

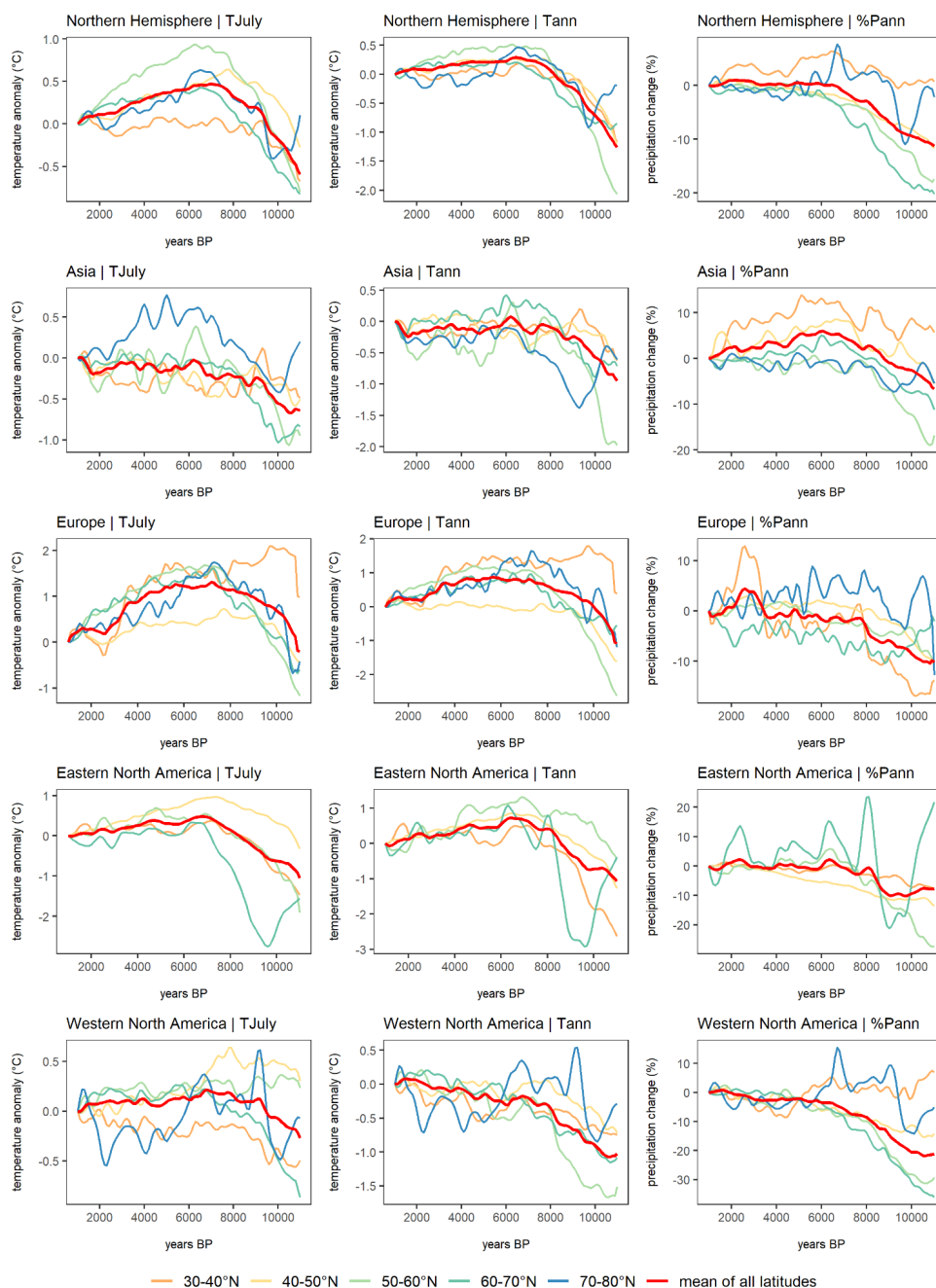
Holocene mean  $P_{ann}$  variations (as % of modern value) averaged across the Northern Hemisphere  
extratropics have patterns that are mostly similar to  $T_{ann}$  with  $P_{ann}$  being lowest during the Early Holocene  
225 (-11.25% at 11 ka compared to 1 ka) and increasing until 6.5 ka before becoming relatively stable (Fig.  
2).

In contrast to the averaged Northern Hemisphere pattern, the (sub-)continental precipitation patterns  
differ from their respective temperature patterns. The mean precipitation time-series of Western North  
America and Europe increases from the early Holocene to the late Holocene; averaged Eastern North  
230 America precipitation varies slightly around modern values; and Asia shows a pronounced maximum  
between 7 and 5 ka.

Time-series maps of latitudinal means and differences (Fig. 3) reveal strong spatial patterns, particularly  
for Asia. The latitudinal mean time-series in Asia show a strong increase toward the mid-Holocene of  
mostly >10%. After ca. 7 ka, certain differences exist: while the 70°N mean shows no clear further trend,  
235 the other mean curves show an optimum which is at least 5% above the late-Holocene minimum.  
Precipitation optima (compared with the late Holocene) are more pronounced and occur later at lower  
latitudes. Furthermore, the 6-1 ka difference maps reveal that the mid-Holocene moisture maximum in  
subtropical Asia was most pronounced in east-central China with many records even showing >50%  
higher values at 6 ka compared to 1 ka (Fig. 3).

240 The Holocene precipitation increase in the other (sub-)continents is particularly strong in the 30-40°N  
bands in subtropical Europe and mid-latitude North America with >13% and >20% precipitation increase  
respectively. In Europe and Western and Eastern North America the records from 70-80°N show an  
early-Holocene precipitation maximum (particularly pronounced in Alaska), which is in contrast to the  
trends in almost all other latitudinal bands.





245

**Figure 2.** Hemispheric, continental, and latitudinal mean curves for  $T_{July}$ ,  $T_{ann}$ , and  $P_{ann}$ . Curves from latitudinal bands that contain less than three grid cells were excluded.



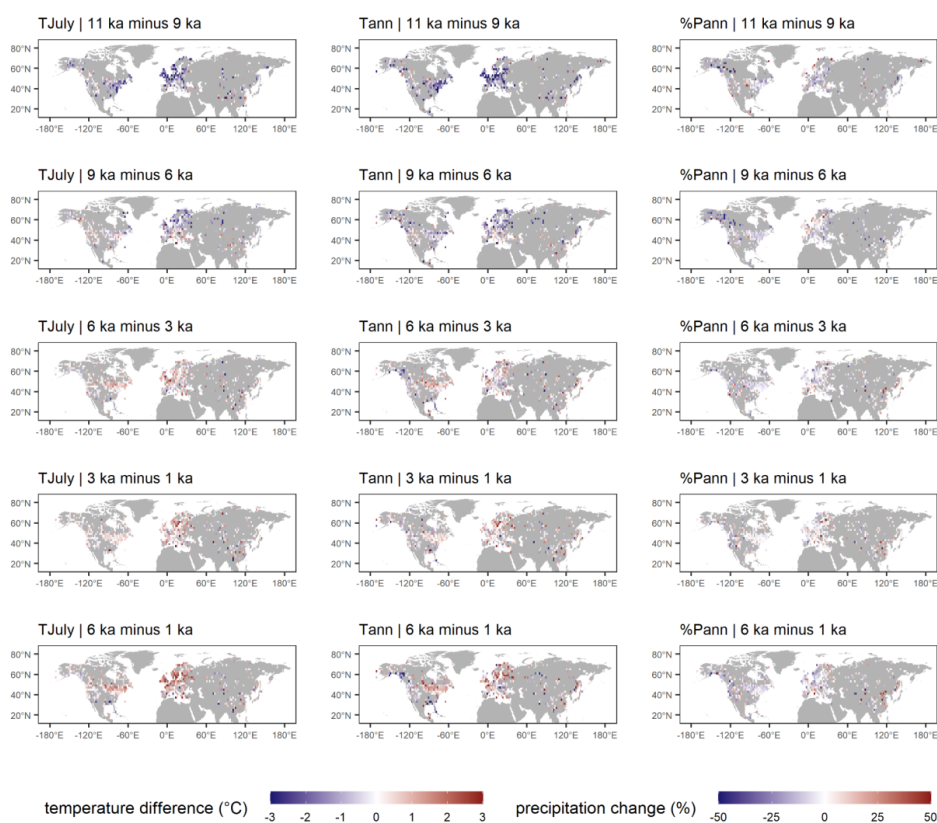


**Figure 3.** Difference maps of  $T_{July}$ ,  $T_{ann}$  ( $^{\circ}C$ ), and  $P_{ann}$  (as % of the value of the younger time-slice) between selected time-slices. Color code for values outside the range were restricted to range maxima. Maps are gridded values averaging the values of records from within the  $2^{\circ} \times 2^{\circ}$  grid-cell.

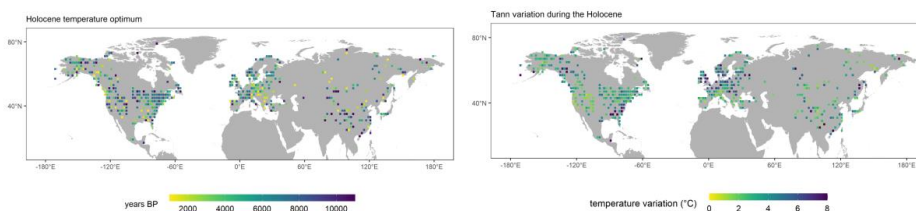
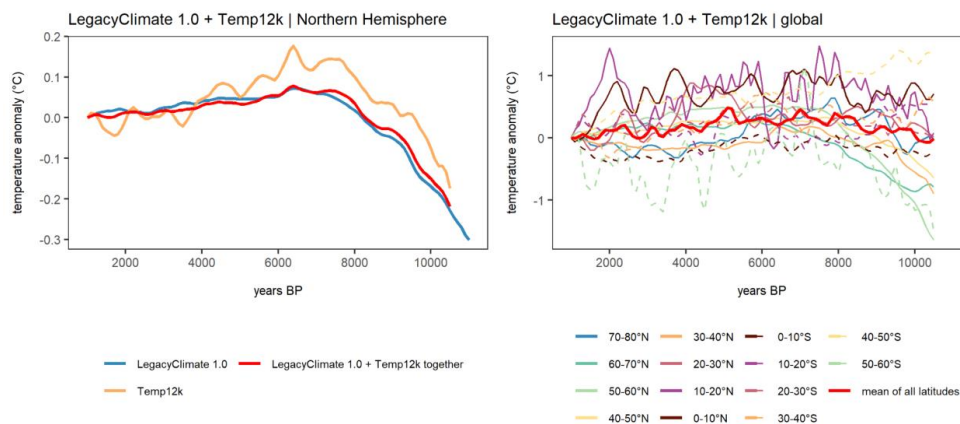


**Figure 4.** Maps indicating the timing of the  $T_{ann}$  optimum (left) and range of  $T_{ann}$  variation during the Holocene (11-1 ka, right). Each  $2^{\circ} \times 2^{\circ}$  grid cell contains the averaged values of all records located within one grid cell. For each grid cell the  $T_{ann}$  variation was determined as the range between minimum and



maximum  $T_{ann}$  anomalies. For  $T_{ann}$  optimum is the timing of the anomaly maximum. Color code for values outside the range were restricted to range maxima.



260

**Figure 5. Mean curves for temperature.** Left: Northern Hemisphere means only (no curves for latitudes): LegacyClimate1.0 (blue), Temp12k dataset (orange, see methods for record filter), LegacyClimate1.0+Temp12k mean (red); right: LegacyClimate1.0+Temp12k mean with latitudinal means.

265

#### 4 Discussion

##### 4.1 Spatial temperature pattern (in light of the global Holocene temperature curve)

The general pattern of the LegacyClimate1.0 mean annual temperature curve of the Northern Hemisphere extratropics agrees with those of previous investigations (Marcott et al., 2013; Kaufman et al., 2020b) including a cold early Holocene, a temperature maximum during the early to mid-Holocene, and a slight cooling towards the present-day. Both our curve and the Temp12k increase about 0.4°C from the early Holocene to the mid-Holocene when the same stacking approach as has been applied to the LegacyClimate 1.0 dataset is applied. However, the LegacyClimate1.0 stack shows only a minimal temperature decline between the early mid-Holocene maximum and the late-Holocene minimum of ~0.07K compared to ~0.18K in the Temp12k stack. We suggest two probable reasons for this finding: 1) a more complete spatial and temporal representativeness of the dataset, and 2) a unique methodology to reconstruct a small set of climate variables from pollen data.

First, our mean annual temperature curve includes about four times the number of records compared with the Temp12k dataset (991 records in the LegacyClimate 1.0 dataset vs. 249 records in the Temp12k dataset, Kaufman et al. 2020b) (Fig. 1a). In particular, Asia is represented by more records in the combined dataset. Our temperature reconstruction from Asia shows an average trend that differs from the overall Northern Hemisphere trend as it has no Holocene optimum. This is particularly true for

280



Asian  $T_{ann}$  records south of  $50^{\circ}N$  and  $T_{July}$  records south of  $60^{\circ}N$ . This feature has not been recognized so far, likely because Asian temperature reconstructions are mostly lacking in previous compilations  
285 (e.g., Marcott et al., 2013; Marsicek et al., 2018; Routson et al., 2019; Kaufman et al., 2020b). Even if the mid-to-late Holocene cooling trend observed in Asia north of  $60^{\circ}N$  agrees with the proposed Neoglacial (sub-)arctic wide Holocene cooling, the amount of cooling of  $<0.5^{\circ}C$  is low compared to the cooling observed in other regions (e.g., in Europe where an average cooling of  $\sim 1.5^{\circ}C$  has been reconstructed; McKay et al., 2018). As with the differences between Eastern and Western Eurasia, we  
290 find a difference between Eastern and Western North America. In particular, we can identify a circum-North Atlantic pattern with a strong early Holocene increase and a pronounced mid-Holocene optimum and strong temperature range, and a circum-North Pacific pattern with an overall weak change. This is likely related to the impact of the decaying Laurentide ice-sheet on the North Atlantic that was probably a stronger driver of early-to-mid Holocene temperature change than insolation (Renssen et al., 2009;  
295 Renssen et al., 2012; Zhang et al., 2016).

Even if this study shows a less pronounced Holocene temperature optimum, the problem remains that this does not align with the overall Holocene increase in the mean global (and Northern Hemisphere) temperature revealed by Earth System Models. Our study points to a strong regionalization of Holocene temperature trends and range of variation in the Northern Hemisphere extratropics. This somehow  
300 contradicts the Holocene conundrum concept which tackled Holocene temperature change mainly from analyzing the Global mean and understanding the differences between proxy-based and simulated reconstructions. Our finding is in line with recent modeling approaches, which also yield strong regional differences in temperature developments (Bader et al., 2020) allowing for a regional comparison. Recent palaeo-data assimilation approaches based on marine temperature reconstructions reveal peculiarities  
305 of spatial averaging as one reason for the model-data mismatch (Osman et al., 2021). The error is most pronounced where the number of included records is small. This stresses the importance of a good spatial coverage of the records used for the assessment of the mean temperature trend. Including terrestrial reconstructions is crucial. Compared with previous syntheses of terrestrial records, our compilation is particularly characterized by a higher record density in Asia, a region for which Earth System Models show diverging past climate changes, highly sensitive to boundary conditions and forcing (Bakker et al. 2020; Brierley et al., 2020; Lohmann et al. 2021). Therefore, our reconstruction makes a decisive contribution to locating and clarifying the model-data mismatch in the Northern Hemisphere extratropics. From a proxy perspective, future targets of synthesis studies should be on the Southern Hemisphere and poorly covered areas in central Asia and Siberia.

315 Second, standardized methodologies may have contributed to the observed differences between LegacyClimate1.0 mean  $T_{ann}$  curve and the Temp12k curve. Our  $T_{ann}$  reconstruction only includes records of mean annual temperature while the Temp12k product mixes reconstructions of seasonal temperature (mostly  $T_{July}$ ) if  $T_{ann}$  is not available from a site. This assumption of equivalence between annual and summer temperature at any given site can impact the trend and amplitude of the stacks. A  
320 seasonal bias in the reconstructions may originate from a real, larger Holocene range of summer temperature variations (Bova et al., 2021) or is an artifact introduced by having a larger  $T_{July}$  range



covered by the calibration datasets compared with  $T_{ann}$  which is, however, not the case in our calibration sets.

Our pollen-based reconstructions are all performed with WA-PLS, which is known to produce smaller  
325 climate amplitudes than MAT (a likewise commonly used method) because it is less sensitive to extreme  
climate values in the modern pollen dataset (Birks and Simpson 2013; Cao et al., 2017; Nolan et al.  
2019). Furthermore, by using a standard area size for our modern pollen datasets, we may have  
stabilized the regional reconstructions, that is, equalized the amplitude as the source areas represent  
rather similar biogeographical and climate ranges. Finally, our reconstructions include only records that  
330 cover the entire Holocene period (11-1 ka) and not just parts of it. Hence, all time-slices have a similar  
spatial coverage and the temporal pattern is not biased by regions where archives are only available in  
certain periods (e.g., the late-Holocene peatland establishment).

As with all applications of taxa-based transfer functions to fossil records, we assume that both modern  
and past taxa assemblages (in our case, vegetation) are in equilibrium with climate, and that the  
335 relationships inferred from modern data do not change throughout the Holocene (Birks et al., 2010;  
Chevalier et al., 2020) and that the modern pollen assemblages are not heavily biased by human impact.  
Differences in global boundary conditions during the early-to-mid Holocene (e.g., lower atmospheric  
 $CO_2$  concentration, different seasonal insolation) however, may have modified these relationships,  
which could have also dampened the reconstructed amplitudes. The absolute effect of these biases is  
340 hard to quantify (but see Cleator et al., 2020), and many comparative, multi-proxy Holocene studies  
have shown that pollen-based reconstructions are as reliable as any other proxy (Kaufmann et al., 2020a;  
Dugerdil et al., 2021). In contrast, one advantage of single proxy studies is that any biases will affect all  
the records similarly. As such, if the actual amplitude of our regional and global stacks might be  
dampened, the trends and spatial patterns shared by the data are likely to remain correct.

345

#### 4.2 Spatio-temporal precipitation pattern

Our analyses of the Holocene spatio-temporal precipitation pattern fill a research gap as syntheses of  
proxy-based precipitation change at the hemispheric scale during the Holocene are still lacking.  
Regional syntheses are available for Europe (Mauri et al., 2014 and 2015), North America (Ladd et al.,  
350 2015; Routson et al., 2021), and Eastern Asia (Herzschuh et al., 2019). Interestingly, we observed a  
similar pattern for Northern Hemisphere-wide averaged Holocene trends of  $P_{ann}$  and  $T_{ann}$  but differences  
among corresponding  $P_{ann}$  and  $T_{ann}$  curves at (sub-)continental and latitudinal scales.

This regional heterogeneity with respect to the precipitation trend is also seen in recent Earth System  
Model simulations for the last 8000 years (Mauri et al., 2014; Dallmeyer et al., 2021). Although the  
355 simulated pattern does not exactly match our reconstructions, they share many similar structures such  
as a pronounced decrease of precipitation in East Asia since the mid-Holocene. For this region, our  
reconstruction shows the strongest mid-to-late Holocene precipitation decline worldwide, reflecting the  
weakening of the East Asian Summer Monsoon (EASM) in response to the decrease in summer  
insolation. This trend in moisture has been confirmed by earlier qualitative and quantitative proxy



360 syntheses and modeling studies (Wang et al., 2010; Zheng et al., 2013; Liu et al., 2014a; Herzsuh et al., 2019).

In contrast, many central Asian sites indicate an increase in precipitation from the early to mid-Holocene. This anti-phase relationship in EASM to central Asian moisture change is in line with earlier studies (Jin et al., 2012; Chen et al., 2019; Herzsuh et al., 2019; Zhang et al., 2021). The causal mechanisms are still debated. Among other reasons, precipitation-evaporation effects (Herzsuh, 2004; Zhang et al., 2011; Kubota et al., 2015), transcending air mass related to the Rodwell-Hoskins response to monsoonal heating (Herzsuh, 2004; Wang et al., 2017), effects from winter precipitation (Li et al., 2020), and translocation of the westerly jetstream (Herzsuh et al., 2019) may contribute to the anti-phased precipitation change.

370 Arctic warming mechanistically should be linked with wetting in the Arctic due to high hydrological sensitivities (Trenberth, 2011). Such a pattern is, for example, obvious for early-to-mid Holocene climate change in most records from Alaska. Interestingly, several records from the northern Arctic coastal region in Russia, northern Norway, and Canada show a wet early Holocene which is also observed in simulations (Dallmeyer et al., 2021).

375 Contrasting the trend in the East Asian monsoon region, annual precipitation increases in mid-latitude Europe during the Holocene according to our reconstructions. Routson et al. (2019) propose a circum-hemispheric mid-latitudinal rise of moisture levels over the Holocene based on a semi-quantitative dataset that is strongly concentrated around the circum-Atlantic region. They relate the decreased net precipitation to the weakened early-Holocene latitudinal temperature gradient. Due to polar amplification, the arctic regions experienced a stronger warming in the climate compared to the equatorial region, which is also confirmed by our dataset. However, we also see in our reconstructions that this view is too general, but it may explain the precipitation response in Europe as the weakening of the latitudinal temperature gradient is particularly pronounced in Europe in our reconstructions. This change in temperature pattern is probably a result of a dampening in the cyclonic activity along the weaker westerly jet (Chang et al., 2002; Routson et al., 2019; Xu et al., 2020), bearing less precipitation during the early Holocene compared to modern conditions. With the strengthening of the latitudinal temperature gradient towards the late Holocene, cyclonic activity enhances, leading to an increase of precipitation over the Holocene.

According to our reconstructions, the precipitation trend in Eastern and Western North America strongly differs (Fig. 2). While in the eastern part the mean precipitation level is relatively stable in all latitudinal bands over the Holocene, precipitation strongly increases on average in the western part, driven by a precipitation rise in the mid-latitudes (40-70°N). In the polar regions and south of 40°N, precipitation declines from the mid-Holocene (Fig. 3). The latter may be related to a decrease in the North American monsoon intensity, in line with the orbital monsoon hypothesis (Kutzbach, 1981; Harrison et al., 2003).

395 In the polar region, modeling studies report northward shifted storm tracks coinciding with a northward replaced upper tropospheric jetstream in the mid-Holocene compared to the late Holocene, promoting precipitation in the arctic region and decreasing precipitation at mid-latitudes (Zhou et al., 2020;



Dallmeyer et al., 2021). With the southward shift of the polar jet during the Holocene, precipitation decreased in the high northern latitudes in North America and increased further south (Liu et al., 2014b).

400 The rise in moisture levels across the North American continental interior over the course of the Holocene has been proposed before (Grimm et al., 2001; Zhou et al., 2020; Dallmeyer et al., 2021) but has not yet been quantified with continental-wide proxy-data. The main drivers of this trend are still being debated: besides shifts in the westerly wind circulation (Seager et al., 2014), weakening subsidence caused by teleconnection with the weakening northern hemispheric monsoon systems (Harrison et al., 405 2003; Dallmeyer et al., 2021), re-organization of the atmospheric circulation around the Bermuda high (Grimm et al., 2001), and changes in the sea-surface temperature pattern (Shin et al., 2006) may contribute to an increase in precipitation over the Holocene.

Reconstructing temperature and precipitation from a single dataset implies that they are both important in defining the presence and/or abundance of specific pollen taxa (Salonen et al., 2019). This hypothesis 410 cannot be tested but to some extent has been assessed by several analyses (Juggins, 2013). The WA-PLS was also applied with tailored modern calibration sets (i.e., selecting samples so that the correlation between temperature and precipitation in the calibration dataset is reduced). The finding that the reconstructions were generally very similar between those using the full and those using the tailored 415 modern datasets can be taken as an indication that co-variation is not a major issue in these reconstructions (Herzschuh et al., 2022a). This conclusion is also supported by the fact that  $T_{ann}$  and  $P_{ann}$  records that pass the reconstruction significance test when the impact of the other variable is partialled out (Telford and Birks, 2011), are almost evenly distributed over the Northern Hemisphere records (Herzschuh et al., 2022a). This is also confirmed by the visual inspection of the regional reconstructions in Fig. 2, where we cannot detect correlations between variables within latitudinal zones, 420 as would be expected from dependent reconstructions. This suggests that our reconstructions do reflect distinctive trends from the pollen data.

## 5 Conclusions

We investigated Holocene time-series of  $T_{July}$ ,  $T_{ann}$ , and  $P_{ann}$  for the Northern Hemisphere extratropics 425 making use of 2594 pollen-based reconstructions (LegacyClimate 1.0). Compared with previous datasets, we include many more records, particularly from Asia. We present mean curves obtained with the same method for the hemisphere, the (sub-)continent (Asia, Europe, Eastern North America, Western North America), and regional zones (i.e.,  $10^\circ$  latitudinal bands for (sub-)continents) as well as Northern Hemisphere gridded data for selected time-slices.

430 Our results indicate that Holocene climate change shows unique regional patterns. The concept of a mid-Holocene temperature optimum only applies mainly to the mid and high northern latitudes in the circum-North Atlantic region while records from mid-latitude Asia, Western North America, and all subtropical areas do not fit into this concept but mostly show an overall Holocene increase or other pattern. As such, the Holocene conundrum concept, originally proposed as a global feature, may instead 435 apply to a restricted region.



The precipitation trend is roughly similar with the temperature trend at the hemispheric scale, in particular with respect to the strong increase from the early to mid-Holocene. At the regional scale, the precipitation trends differ from each other and also from the regional temperature trends. The 30-40° latitudinal band in Asia shows the most pronounced mid-Holocene precipitation optima while many regions show increasing Holocene trends including most of Europe and Western North America. We relate these differences to regionally specific circulation mechanisms and their specific relationships with temperature changes.

Given a background of strong regional heterogeneity, the calculation of global or hemispheric means might generally lead to misleading concepts but focus should be on understanding the spatio-temporal patterns requiring spatially dense proxy-datasets for comparison with simulations.

## 6 Data Availability

The compilation of reconstructed  $T_{July}$ ,  $T_{ann}$ , and  $P_{ann}$ , is open access and available at PANGAEA (<https://doi.pangaea.de/10.1594/PANGAEA.930512>; in the “Other version” section). The dataset files are stored in machine-readable data format (.CSV), which are already separated into Western North America, Eastern North America, Europe, and Asia for easy access and use.

**Author contributions.** UH designed the study. The analyses were led by UH and implemented by TB. UH guided the interpretation of the results and collected detailed comments from AD, MC, OP, CL, and RH. All co-authors commented on the initial version of the manuscript.

**Competing interests.** The authors declare that they have no conflict of interest.

**Acknowledgements.** We would like to express our gratitude to all the palynologists and geologists who, either directly or indirectly by providing their work the Neotoma Paleocology Database, contributed pollen data and chronologies to the dataset. The work of data contributors, data stewards, and the Neotoma community is gratefully acknowledged. We also thank Cathy Jenks for language editing.

**Financial support.** This research has been supported by the European Research Council (ERC Glacial Legacy 772852 to UH) and the PalMod Initiative (01LP1510C to UH). TB, MC, and AD are supported by the German Federal Ministry of Education and Research (BMBF) as a Research for Sustainability initiative (FONA; <https://www.fona.de/en>) through the PalMod Phase II project (grant no. FKZ: 01LP1926D and 01LP1920A). CL holds a scholarship from the Chinese Scholarship Council (grant no. 201908130165). NR work was supported by the Russian Science Foundation (Grant No. 20-17-00110).

470





## References

- Bader, J., Jungclaus, J., Krivova, N., Lorenz, S., Maycock, A., Raddatz, T., Schmidt, H., Toohey, M., Wu, C.-J., and Claussen, M.: Global temperature modes shed light on the Holocene temperature conundrum, *Nat. Commun.*, 11, 4726, <https://doi.org/10.1038/s41467-020-18478-6>, 2020.
- 475 Bakker, P., Rogozhina, I., Merkel, U., and Prange, M.: Hypersensitivity of glacial summer temperatures in Siberia, *Clim. Past*, 16, 371–386, <https://doi.org/10.5194/cp-16-371-2020>, 2020.
- Birks, H. J. B., Heiri, O., Seppä, H., and Bjune, A. E.: Strengths and Weaknesses of Quantitative Climate Reconstructions Based on Late-Quaternary, *Open Ecol. J.*, 3, <http://dx.doi.org/10.2174/1874213001003020068>, 2010.
- 480 Birks, H. J. B. and Simpson, G. L.: 'Diatoms and pH reconstruction' (1990) revisited, *J. Paleolimnol.*, 49, 363–371, <https://doi.org/10.1007/s10933-013-9697-7>, 2013.
- Bova, S., Rosenthal, Y., Liu, Z., Godad, S. P., and Yan, M.: Seasonal origin of the thermal maxima at the Holocene and the last interglacial, *Nature*, 589, 548–553, <https://doi.org/10.1038/s41586-020-03155-x>, 2021.
- 485 ter Braak, C. J. F. and Juggins, S.: Weighted averaging partial least squares regression (WA-PLS): an improved method for reconstructing environmental variables from species assemblages, *Hydrobiologia*, 269, 485–502, <https://doi.org/10.1007/BF00028046>, 1993.
- Brierley, C. M., Zhao, A., Harrison, S. P., Braconnot, P., Williams, C. J. R., Thornalley, D. J. R., Shi, X., Peterschmitt, J.-Y., Ohgaito, R., Kaufman, D. S., Kageyama, M., Hargreaves, J. C., Erb, M. P., Emile-Geay, J., D'Agostino, R., Chandan, D., Carré, M., Bartlein, P. J., Zheng, W., Zhang, Z., Zhang, Q., Yang, H., Volodin, E. M., Tomas, R. A., Routson, C., Peltier, W. R., Otto-Bliesner, B., Morozova, P. A., McKay, N. P., Lohmann, G., Legrande, A. N., Guo, C., Cao, J., Brady, E., Annan, J. D., and Abe-Ouchi, A.: Large-scale features and evaluation of the PMIP4-CMIP6 midHolocene simulations, *Clim. Past*, 16, 1847–1872, <https://doi.org/10.5194/cp-16-1847-2020>, 2020.
- 495 Cao, X., Ni, J., Herzschuh, U., Wang, Y., and Zhao, Y.: A late Quaternary pollen dataset from eastern continental Asia for vegetation and climate reconstructions: Set up and evaluation, *Rev. Palaeobot. Palynol.*, 194, 21–37, <https://doi.org/10.1016/j.revpalbo.2013.02.003>, 2013.
- Cao, X., Herzschuh, U., Telford, R. J., and Ni, J.: A modern pollen–climate dataset from China and Mongolia: Assessing its potential for climate reconstruction, *Rev. Palaeobot. Palynol.*, 211, 87–96, <https://doi.org/10.1016/j.revpalbo.2014.08.007>, 2014.
- 500 Cao, X., Tian, F., Dallmeyer, A., and Herzschuh, U.: Northern Hemisphere biome changes (>30°N) since 40 cal ka BP and their driving factors inferred from model-data comparisons, *Quat. Sci. Rev.*, 220, 291–309, <https://doi.org/10.1016/j.quascirev.2019.07.034>, 2019.



- 505 Cao, X., Tian, F., Telford, R. J., Ni, J., Xu, Q., Chen, F., Liu, X., Stebich, M., Zhao, Y., and Herzschuh, U.: Impacts of the spatial extent of pollen-climate calibration-set on the absolute values, range and trends of reconstructed Holocene precipitation, *Quat. Sci. Rev.*, 178, 37–53, <https://doi.org/10.1016/j.quascirev.2017.10.030>, 2017.
- Chang, E. K. M., Lee, S., and Swanson, K. L.: Storm Track Dynamics, *J. Clim.*, 15, 2163–2183, [https://doi.org/10.1175/1520-0442\(2002\)015<02163:STD>2.0.CO;2](https://doi.org/10.1175/1520-0442(2002)015<02163:STD>2.0.CO;2), 2002.
- 510 Chen, F., Xu, Q., Chen, J., Birks, H. J. B., Liu, J., Zhang, S., Jin, L., An, C., Telford, R. J., Cao, X., Wang, Z., Zhang, X., Selvaraj, K., Lu, H., Li, Y., Zheng, Z., Wang, H., Zhou, A., Dong, G., Zhang, J., Huang, X., Bloemendal, J., and Rao, Z.: East Asian summer monsoon precipitation variability since the last deglaciation, *Sci. Rep.*, 5, 11186, <https://doi.org/10.1038/srep11186>, 2015.
- 515 Chen, F., Chen, J., Huang, W., Chen, S., Huang, X., Jin, L., Jia, J., Zhang, X., An, C., Zhang, J., Zhao, Y., Yu, Z., Zhang, R., Liu, J., Zhou, A., and Feng, S.: Westerlies Asia and monsoonal Asia: Spatiotemporal differences in climate change and possible mechanisms on decadal to sub-orbital timescales, *Earth Sci. Rev.*, 192, 337–354, <https://doi.org/10.1016/j.earscirev.2019.03.005>, 2019.
- 520 Chevalier, M., Davis, B. A. S., Heiri, O., Seppä, H., Chase, B. M., Gajewski, K., Lacourse, T., Telford, R. J., Finsinger, W., Guiot, J., Kühl, N., Maezumi, S. Y., Tipton, J. R., Carter, V. A., Brussel, T., Phelps, L. N., Dawson, A., Zanon, M., Vallé, F., Nolan, C., Mauri, A., de Vernal, A., Izumi, K., Holmström, L., Marsicek, J., Goring, S., Sommer, P. S., Chaput, M., and Kupriyanov, D.: Pollen-based climate reconstruction techniques for late Quaternary studies, *Earth Sci. Rev.*, 210, 103384, <https://doi.org/10.1016/j.earscirev.2020.103384>, 2020.
- 525 Chouinard, C. and Mareschal, J.-C.: Ground surface temperature history in southern Canada: Temperatures at the base of the Laurentide ice sheet and during the Holocene, *Earth Planet. Sci. Lett.*, 277, 280–289, <https://doi.org/10.1016/j.epsl.2008.10.026>, 2009.
- Cleator, S. F., Harrison, S. P., Nichols, N. K., Prentice, I. C., and Roulstone, I.: A new multivariable benchmark for Last Glacial Maximum climate simulations, *Clim. Past*, 16, 699–712, <https://doi.org/10.5194/cp-16-699-2020>, 2020.
- 530 Dallmeyer, A., Claussen, M., Lorenz, S. J., Sigl, M., Toohey, M., and Herzschuh, U.: Holocene vegetation transitions and their climatic drivers in MPI-ESM1.2, *Clim. Past*, 17, 2481–2513, <https://doi.org/10.5194/cp-17-2481-2021>, 2021.
- 535 Davis, B. A. S., Brewer, S., Stevenson, A. C., and Guiot, J.: The temperature of Europe during the Holocene reconstructed from pollen data, *Quat. Sci. Rev.*, 22, 1701–1716, [https://doi.org/10.1016/S0277-3791\(03\)00173-2](https://doi.org/10.1016/S0277-3791(03)00173-2), 2003.
- Davis, B. A. S., Chevalier, M., Sommer, P., Carter, V. A., Finsinger, W., Mauri, A., Phelps, L. N., Zanon, M., Abegglen, R., Åkesson, C. M., Alba-Sánchez, F., Anderson, R. S., Antipina, T. G., Atanassova, J.



- R., Beer, R., Belyanina, N. I., Blyakharchuk, T. A., Borisova, O. K., Bozilova, E., Bukreeva, G., Bunting, M. J., Clò, E., Colombaroli, D., Combourieu-Nebout, N., Desprat, S., Di Rita, F., Djamali, M., Edwards, K. J., Fall, P. L., Feurdean, A., Fletcher, W., Florenzano, A., Furlanetto, G., Gaceur, E., Galimov, A. T., Gałka, M., García-Moreiras, I., Giesecke, T., Grindean, R., Guido, M. A., Gvozdeva, I. G., Herzsuh, U., Hjelle, K. L., Ivanov, S., Jahns, S., Jankovska, V., Jiménez-Moreno, G., Karpińska-Kolaczek, M., Kitaba, I., Kolaczek, P., Lapteva, E. G., Latałowa, M., Lebreton, V., Leroy, S., Leydet, M., Lopatina, D. A., López-Sáez, J. A., Lotter, A. F., Magri, D., Marinova, E., Matthias, I., Mavridou, A., Mercuri, A. M., Mesa-Fernández, J. M., Mikishin, Y. A., Milecka, K., Montanari, C., Morales-Molino, C., Mrotzek, A., Muñoz Sobrino, C., Naidina, O. D., Nakagawa, T., Nielsen, A. B., Novenko, E. Y., Panajiotidis, S., Panova, N. K., Papadopoulou, M., Pardoe, H. S., Pędziszewska, A., Petrenko, T. I., Ramos-Román, M. J., Ravazzi, C., Rösch, M., Ryabogina, N., Sabariego Ruiz, S., Salonen, J. S., Sapelko, T. V., Schofield, J. E., Seppä, H., Shumilovskikh, L., Stivrins, N., Stojakowits, P., Svobodova Svitavská, H., Święta-Musznicka, J., Tantau, I., Tinner, W., Tobolski, K., Tonkov, S., Tsakiridou, M., et al.: The Eurasian Modern Pollen Database (EMPD), version 2, *Earth Syst. Sci. Data*, 12, 2423–2445, <https://doi.org/10.5194/essd-12-2423-2020>, 2020.
- Dugerdil, L., Joannin, S., Peyron, O., Jouffroy-Bapicot, I., Vannièrè, B., Boldgiv, B., Unkelbach, J., Behling, H., and Ménot, G.: Climate reconstructions based on GDGT and pollen surface datasets from Mongolia and Baikal area: calibrations and applicability to extremely cold–dry environments over the Late Holocene, *Clim. Past*, 17, 1199–1226, <https://doi.org/10.5194/cp-17-1199-2021>, 2021.
- Fick, S. E. and Hijmans, R. J.: WorldClim 2: new 1-km spatial resolution climate surfaces for global land areas, *Int. J. Climatol.*, 37, 4302–4315, <https://doi.org/10.1002/joc.5086>, 2017.
- Grimm, E. C., Lozano-García, S., Behling, H., and Markgraf, V.: Chapter 19 - Holocene Vegetation and Climate Variability in the Americas, in: *Interhemispheric Climate Linkages*, edited by: Markgraf, V., Academic Press, San Diego, 325–370, <https://doi.org/10.1016/B978-012472670-3/50022-7>, 2001.
- Harrison, S. P., Kutzbach, J. E., Liu, Z., Bartlein, P. J., Otto-Bliesner, B., Muhs, D., Prentice, I. C., and Thompson, R. S.: Mid-Holocene climates of the Americas: a dynamical response to changed seasonality, *Clim. Dyn.*, 20, 663–688, <https://doi.org/10.1007/s00382-002-0300-6>, 2003.
- Herzsuh, U., Tarasov, P., Wünnemann, B., and Hartmann, K.: Holocene vegetation and climate of the Alashan Plateau, NW China, reconstructed from pollen data, *Palaeogeogr. Palaeoclimatol. Palaeoecol.*, 211, 1–17, <https://doi.org/10.1016/j.palaeo.2004.04.001>, 2004.
- Herzsuh, U., Cao, X., Laepple, T., Dallmeyer, A., Telford, R. J., Ni, J., Chen, F., Kong, Z., Liu, G., Liu, K.-B., Liu, X., Stebich, M., Tang, L., Tian, F., Wang, Y., Wischnowski, J., Xu, Q., Yan, S., Yang, Z., Yu, G., Zhang, Y., Zhao, Y., and Zheng, Z.: Position and orientation of the westerly jet determined Holocene rainfall patterns in China, *Nat. Commun.*, 10, 2376, <https://doi.org/10.1038/s41467-019-09866-8>, 2019.



Herzschuh, U., Böhmer, T., Li, C., and Cao, X.: Northern Hemisphere temperature and precipitation reconstruction from taxonomically harmonized pollen data set with revised chronologies using WA-PLS and MAT (LegacyClimate 1.0), PANGAEA, <https://doi.pangaea.de/10.1594/PANGAEA.930512>, 2021.

575 Herzschuh, U., Böhmer, T., Li, C., Chevalier, M., Dallmeyer, A., Cao, X., Bigelow, N. H., Nazarova, L., Novenko, E. Y., Park, J., Peyron, O., Rudaya, N. A., Schlütz, F., Shumilovskikh, L. S., Tarasov, P. E., Wang, Y., Wen, R., Xu, Q., and Zheng, Z.: LegacyClimate 1.0: A dataset of pollen-based climate reconstructions from 2594 Northern Hemisphere sites covering the late Quaternary, *Earth Syst. Sci. Data*, 1–29, <https://doi.org/10.5194/essd-2022-38>, 2022a.

580 Herzschuh, U., Li, C., Böhmer, T., Postl, A. K., Heim, B., Andreev, A. A., Cao, X., Wieczorek, M., and Ni, J.: LegacyPollen 1.0: A taxonomically harmonized global Late Quaternary pollen dataset of 2831 records with standardized chronologies, *Earth Syst. Sci. Data*, 1–25, <https://doi.org/10.5194/essd-2022-37>, 2022b.

Hijmans, R. J., van Etten, J., Sumner, M., Cheng, J., Baston, D., Bevan, A., Bivand, R., Busetto, L., Canty, M., Fasoli, B., Forrest, D., Ghosh, A., Golicher, D., Gray, J., Greenberg, J. A., Hiemstra, P., Hingee, K., Ilich, A., Institute for Mathematics Applied Geosciences, Karney, C., Mattiuzzi, M., Mosher, S., Naimi, B., Nowosad, J., Pebesma, E., Lamigueiro, O. P., Racine, E. B., Rowlingson, B., Shortridge, A., Venables, B., and Wueest, R.: Raster: Geographic Data Analysis and Modeling, R package version 3.5-11, <https://cran.r-project.org/web/packages/raster>, 2021.

590 Jin, L., Chen, F., Morrill, C., Otto-Bliesner, B. L., and Rosenbloom, N.: Causes of early Holocene desertification in arid central Asia, *Clim. Dyn.*, 38, 1577–1591, <https://doi.org/10.1007/s00382-011-1086-1>, 2012.

Juggins, S.: Quantitative reconstructions in palaeolimnology: new paradigm or sick science?, *Quat. Sci. Rev.*, 64, 20–32, <https://doi.org/10.1016/j.quascirev.2012.12.014>, 2013.

595 Kaufman, D., McKay, N., Routson, C., Erb, M., Davis, B., Heiri, O., Jaccard, S., Tierney, J., Dätwyler, C., Axford, Y., Brussel, T., Cartapanis, O., Chase, B., Dawson, A., de Vernal, A., Engels, S., Jonkers, L., Marsicek, J., Moffa-Sánchez, P., Morrill, C., Orsi, A., Rehfeld, K., Saunders, K., Sommer, P. S., Thomas, E., Tonello, M., Tóth, M., Vachula, R., Andreev, A., Bertrand, S., Biskaborn, B., Bringué, M., Brooks, S., Caniupán, M., Chevalier, M., Cwynar, L., Emile-Geay, J., Fegyveresi, J., Feurdean, A., Finsinger, W., Fortin, M.-C., Foster, L., Fox, M., Gajewski, K., Grosjean, M., Hausmann, S., Heinrichs, M., Holmes, N., Ilyashuk, B., Ilyashuk, E., Juggins, S., Khider, D., Koinig, K., Langdon, P., Larocque-Tobler, I., Li, J., Lotter, A., Luoto, T., Mackay, A., Magyari, E., Malevich, S., Mark, B., Massaferró, J., Montade, V., Nazarova, L., Novenko, E., Pařil, P., Pearson, E., Peros, M., Pienitz, R., Plóciennik, M., Porinchu, D., Potito, A., Rees, A., Reinemann, S., Roberts, S., Rolland, N., Salonen, S., Self, A., Seppä, H., Shala, S., St-Jacques, J.-M., Stenni, B., Syrykh, L., Tarrats, P., Taylor, K., van den Bos, V., Velle, G., Wahl, E., Walker, I., Wilmshurst, J., Zhang, E., and Zhilich, S.: A global database of Holocene paleotemperature records, *Sci. Data*, 7, 115, <https://doi.org/10.1038/s41597-020-0445-3>, 2020a.



- 610 Kaufman, D., McKay, N., Routsos, C., Erb, M., Dätwyler, C., Sommer, P. S., Heiri, O., and Davis, B.: Holocene global mean surface temperature, a multi-method reconstruction approach, *Sci. Data*, 7, 201, <https://doi.org/10.1038/s41597-020-0530-7>, 2020b.
- Kubota, Y., Tada, R., and Kimoto, K.: Changes in East Asian summer monsoon precipitation during the Holocene deduced from a freshwater flux reconstruction of the Changjiang (Yangtze River) based on the oxygen isotope mass balance in the northern East China Sea, *Clim. Past*, 11, 265–281, <https://doi.org/10.5194/cp-11-265-2015>, 2015.
- 615 Kutzbach, J. E.: Monsoon Climate of the Early Holocene: Climate Experiment with the Earth's Orbital Parameters for 9000 Years Ago, *Science*, <https://doi.org/10.1126/science.214.4516.59>, 1981.
- Ladd, M., Way, R. G., and Viau, A. E.: The impact of using different modern climate data sets in pollen-based paleoclimate reconstructions of North America, *Quat. Sci. Rev.*, 112, 78–85, <https://doi.org/10.1016/j.quascirev.2015.01.020>, 2015.
- 620 Li, C., Postl, A. K., Böhmer, T., Cao, X., Dolman, A. M., and Herzschuh, U.: Harmonized chronologies of a global late Quaternary pollen dataset (LegacyAge 1.0), *Earth Syst. Sci. Data*, 14, 1331–1343, <https://doi.org/10.5194/essd-14-1331-2022>, 2022.
- Li, J., Wang, N., Dodson, J., Yan, H., Zhang, X., Jia, P. W., and Seppä, H.: Holocene negative coupling of summer temperature and moisture availability over southeastern arid Central Asia, *Clim. Dyn.*, 55, 1187–1208, <https://doi.org/10.1007/s00382-020-05319-x>, 2020.
- 625 Liu, Z., Wen, X., Brady, E. C., Otto-Bliesner, B., Yu, G., Lu, H., Cheng, H., Wang, Y., Zheng, W., Ding, Y., Edwards, R. L., Cheng, J., Liu, W., and Yang, H.: Chinese cave records and the East Asia Summer Monsoon, *Quat. Sci. Rev.*, 83, 115–128, <https://doi.org/10.1016/j.quascirev.2013.10.021>, 2014a.
- Liu, Z., Yoshimura, K., Bowen, G. J., Buening, N. H., Risi, C., Welker, J. M., and Yuan, F.: Paired oxygen isotope records reveal modern North American atmospheric dynamics during the Holocene, *Nat. Commun.*, 5, 3701, <https://doi.org/10.1038/ncomms4701>, 2014b.
- 630 Liu, Z., Zhu, J., Rosenthal, Y., Zhang, X., Otto-Bliesner, B. L., Timmermann, A., Smith, R. S., Lohmann, G., Zheng, W., and Timm, O. E.: The Holocene temperature conundrum, *PNAS*, 111, E3501–E3505, <https://doi.org/10.1073/pnas.1407229111>, 2014c.
- 635 Lohmann, G., Wagner, A., and Prange, M.: Resolution of the atmospheric model matters for the Northern Hemisphere Mid-Holocene climate, *Dyn. Atmospheres Oceans*, 93, 101206, <https://doi.org/10.1016/j.dynatmoce.2021.101206>, 2021.
- Marcott, S. A., Shakun, J. D., Clark, P. U., and Mix, A. C.: A Reconstruction of Regional and Global Temperature for the Past 11,300 Years, *Science*, <https://doi.org/10.1126/science.1228026>, 2013.



- 640 Marsicek, J., Shuman, B. N., Bartlein, P. J., Shafer, S. L., and Brewer, S.: Reconciling divergent trends and millennial variations in Holocene temperatures, *Nature*, 554, 92–96, <https://doi.org/10.1038/nature25464>, 2018.
- Mauri, A., Davis, B. a. S., Collins, P. M., and Kaplan, J. O.: The influence of atmospheric circulation on the mid-Holocene climate of Europe: a data–model comparison, *Clim. Past*, 10, 1925–1938, 645 <https://doi.org/10.5194/cp-10-1925-2014>, 2014.
- Mauri, A., Davis, B. A. S., Collins, P. M., and Kaplan, J. O.: The climate of Europe during the Holocene: a gridded pollen-based reconstruction and its multi-proxy evaluation, *Quat. Sci. Rev.*, 112, 109–127, <https://doi.org/10.1016/j.quascirev.2015.01.013>, 2015.
- McKay, N. P., Kaufman, D. S., Routson, C. C., Erb, M. P., and Zander, P. D.: The Onset and Rate of 650 Holocene Neoglacial Cooling in the Arctic, *Geophys. Res. Lett.*, 45, 12,487–12,496, <https://doi.org/10.1029/2018GL079773>, 2018.
- Nolan, C., Tipton, J., Booth, R. K., Hooten, M. B., and Jackson, S. T.: Comparing and improving methods for reconstructing peatland water-table depth from testate amoebae, *Holocene*, 29, 1350–1361, <https://doi.org/10.1177/0959683619846969>, 2019.
- 655 Osman, M. B., Tierney, J. E., Zhu, J., Tardif, R., Hakim, G. J., King, J., and Poulsen, C. J.: Globally resolved surface temperatures since the Last Glacial Maximum, *Nature*, 599, 239–244, <https://doi.org/10.1038/s41586-021-03984-4>, 2021.
- R Core Team: R: A language and environment for statistical computing, R Foundation for Statistical Computing, Vienna, Austria, <https://www.r-project.org/>, 2020.
- 660 Renssen, H., Seppä, H., Heiri, O., Roche, D. M., Goosse, H., and Fichet, T.: The spatial and temporal complexity of the Holocene thermal maximum, *Nat. Geosci.*, 2, 411–414, <https://doi.org/10.1038/ngeo513>, 2009.
- Renssen, H., Seppä, H., Crosta, X., Goosse, H., and Roche, D. M.: Global characterization of the Holocene Thermal Maximum, *Quat. Sci. Rev.*, 48, 7–19, 665 <https://doi.org/10.1016/j.quascirev.2012.05.022>, 2012.
- Reschke, M., Kunz, T., and Laepple, T.: Comparing methods for analysing time scale dependent correlations in irregularly sampled time series data, *Comput. Geosci.*, 123, 65–72, <https://doi.org/10.1016/j.cageo.2018.11.009>, 2019.
- Rolandone, F., Mareschal, J.-C., and Jaupart, C.: Temperatures at the base of the Laurentide Ice Sheet 670 inferred from borehole temperature data, *Geophys. Res. Lett.*, 30, <https://doi.org/10.1029/2003GL018046>, 2003.



Routson, C. C., McKay, N. P., Kaufman, D. S., Erb, M. P., Goosse, H., Shuman, B. N., Rodysill, J. R., and Ault, T.: Mid-latitude net precipitation decreased with Arctic warming during the Holocene, *Nature*, 568, 83–87, <https://doi.org/10.1038/s41586-019-1060-3>, 2019.

675 Routson, C. C., Kaufman, D. S., McKay, N. P., Erb, M. P., Arcusa, S. H., Brown, K. J., Kirby, M. E., Marsicek, J. P., Anderson, R. S., Jiménez-Moreno, G., Rodysill, J. R., Lachniet, M. S., Fritz, S. C., Bennett, J. R., Goman, M. F., Metcalfe, S. E., Galloway, J. M., Schoups, G., Wahl, D. B., Morris, J. L., Staines-Urías, F., Dawson, A., Shuman, B. N., Gavin, D. G., Munroe, J. S., and Cumming, B. F.: A multiproxy database of western North American Holocene paleoclimate records, *Earth Syst. Sci. Data*, 680 13, 1613–1632, <https://doi.org/10.5194/essd-13-1613-2021>, 2021.

Salonen, J. S., Korpela, M., Williams, J. W., and Luoto, M.: Machine-learning based reconstructions of primary and secondary climate variables from North American and European fossil pollen data, *Sci. Rep.*, 9, 15805, <https://doi.org/10.1038/s41598-019-52293-4>, 2019.

685 Seager, R., Neelin, D., Simpson, I., Liu, H., Henderson, N., Shaw, T., Kushnir, Y., Ting, M., and Cook, B.: Dynamical and Thermodynamical Causes of Large-Scale Changes in the Hydrological Cycle over North America in Response to Global Warming, *J. Clim.*, 27, 7921–7948, <https://doi.org/10.1175/JCLI-D-14-00153.1>, 2014.

Shin, S.-I., Sardeshmukh, P. D., Webb, R. S., Oglesby, R. J., and Barsugli, J. J.: Understanding the Mid-Holocene Climate, *J. Clim.*, 19, 2801–2817, <https://doi.org/10.1175/JCLI3733.1>, 2006.

690 Simpson, G. L.: Analogue Methods in Palaeolimnology, in: *Tracking Environmental Change Using Lake Sediments: Data Handling and Numerical Techniques*, edited by: Birks, H. J. B., Lotter, A. F., Juggins, S., and Smol, J. P., Springer Netherlands, Dordrecht, 495–522, [https://doi.org/10.1007/978-94-007-2745-8\\_15](https://doi.org/10.1007/978-94-007-2745-8_15), 2012.

695 Tarasov, P. E., Nakagawa, T., Demske, D., Österle, H., Igarashi, Y., Kitagawa, J., Mokhova, L., Bazarova, V., Okuda, M., Gotanda, K., Miyoshi, N., Fujiki, T., Takemura, K., Yonenobu, H., and Fleck, A.: Progress in the reconstruction of Quaternary climate dynamics in the Northwest Pacific: A new modern analogue reference dataset and its application to the 430-kyr pollen record from Lake Biwa, *Earth Sci. Rev.*, 108, 64–79, <https://doi.org/10.1016/j.earscirev.2011.06.002>, 2011.

700 Telford, R. J. and Birks, H. J. B.: A novel method for assessing the statistical significance of quantitative reconstructions inferred from biotic assemblages, *Quat. Sci. Rev.*, 30, 1272–1278, <https://doi.org/10.1016/j.quascirev.2011.03.002>, 2011.

Trenberth, K. E.: Changes in precipitation with climate change, *Clim. Res.*, 47, 123–138, <https://doi.org/10.3354/cr00953>, 2011.





- Wang, N., Jiang, D., and Lang, X.: Mechanisms for Spatially Inhomogeneous Changes in East Asian  
705 Summer Monsoon Precipitation during the Mid-Holocene, *J. Clim.*, 33, 2945–2965,  
<https://doi.org/10.1175/JCLI-D-19-0565.1>, 2020.
- Wang, Y., Liu, X., and Herzschuh, U.: Asynchronous evolution of the Indian and East Asian Summer  
Monsoon indicated by Holocene moisture patterns in monsoonal central Asia, *Earth Sci. Rev.*, 103, 135–  
153, <https://doi.org/10.1016/j.earscirev.2010.09.004>, 2010.
- 710 Wang, Y., Bekeschus, B., Handorf, D., Liu, X., Dallmeyer, A., and Herzschuh, U.: Coherent tropical-  
subtropical Holocene see-saw moisture patterns in the Eastern Hemisphere monsoon systems, *Quat.*  
*Sci. Rev.*, 169, 231–242, <https://doi.org/10.1016/j.quascirev.2017.06.006>, 2017.
- Whitmore, J., Gajewski, K., Sawada, M., Williams, J. W., Shuman, B., Bartlein, P. J., Minckley, T., Viau,  
A. E., Webb, T., Shafer, S., Anderson, P., and Brubaker, L.: Modern pollen data from North America  
715 and Greenland for multi-scale paleoenvironmental applications, *Quat. Sci. Rev.*, 24, 1828–1848,  
<https://doi.org/10.1016/j.quascirev.2005.03.005>, 2005.
- Williams, J. W., Webb III, T., Richard, P. H., and Newby, P.: Late Quaternary biomes of Canada and the  
eastern United States, *J. Biogeogr.*, 27, 585–607, <https://doi.org/10.1046/j.1365-2699.2000.00428.x>,  
2000.
- 720 Xu, C., Yan, M., Ning, L., and Liu, J.: Summer Westerly Jet in Northern Hemisphere during the Mid-  
Holocene: A Multi-Model Study, *Atmos.*, 11, 1193, <https://doi.org/10.3390/atmos11111193>, 2020.
- Zhang, J., Chen, F., Holmes, J. A., Li, H., Guo, X., Wang, J., Li, S., Lü, Y., Zhao, Y., and Qiang, M.:  
Holocene monsoon climate documented by oxygen and carbon isotopes from lake sediments and peat  
bogs in China: a review and synthesis, *Quat. Sci. Rev.*, 30, 1973–1987,  
725 <https://doi.org/10.1016/j.quascirev.2011.04.023>, 2011.
- Zhang, Y., Renssen, H., and Seppä, H.: Effects of melting ice sheets and orbital forcing on the early  
Holocene warming in the extratropical Northern Hemisphere, *Clim. Past*, 12, 1119–1135,  
<https://doi.org/10.5194/cp-12-1119-2016>, 2016.
- Zhang, Z., Liu, J., Chen, J., Chen, S., Shen, Z., Chen, J., Liu, X., Wu, D., Sheng, Y., and Chen, F.:  
730 Holocene climatic optimum in the East Asian monsoon region of China defined by climatic stability, *Earth*  
*Sci. Rev.*, 212, 103450, <https://doi.org/10.1016/j.earscirev.2020.103450>, 2021.
- Zheng, W., Wu, B., He, J., and Yu, Y.: The East Asian Summer Monsoon at mid-Holocene: results from  
PMIP3 simulations, *Clim. Past*, 9, 453–466, <https://doi.org/10.5194/cp-9-453-2013>, 2013.
- Zhou, P., Shi, Z., Li, X., and Zhou, W.: Response of Westerly Jet Over the Northern Hemisphere to  
735 Astronomical Insolation During the Holocene, *Front. Earth Sci.*, 8,  
<https://doi.org/10.3389/feart.2020.00282>, 2020.